

Charge driven piezoelectric actuators for structural vibration control: issues and implementation

B J G Vautier and S O R Moheimani

School of Electrical Engineering and Computer Science, The University of Newcastle, Callaghan 2308, NSW, Australia

E-mail: reza@ee.newcastle.edu.au

Received 1 March 2004, in final form 22 November 2004

Published 15 June 2005

Online at stacks.iop.org/SMS/14/575

Abstract

Piezoelectric actuators have been traditionally driven by voltage amplifiers. When driven at large voltages these actuators exhibit a significant amount of distortion, known as hysteresis, which may reduce the stability robustness of the system in feedback control applications. Electric charge is known to reduce the effects of this nonlinearity. To date little research has been done on the coupling between piezoelectric actuators and highly resonant structures when charge is used to drive the actuator. This arrangement was used in a control feedback scheme to reject disturbance vibrations acting on a cantilevered beam. During the analysis it is shown that the dynamics for the coupled ‘piezoelectric–beam’ system differs depending on whether voltage or charge is used to drive the piezoelectric actuator. Experimental results demonstrating the effectiveness of using electrical charge are included.

1. Introduction

Piezoelectric transducers have become increasingly popular in vibration control applications as they provide excellent actuation and sensing capabilities. These properties were discovered more than a hundred years ago by the Curie brothers who found that when a strain is applied to a piezoelectric material a resulting electric charge is produced (this is often referred to as the ‘direct effect’), and conversely an applied electric field results in a strain (also known as the ‘converse effect’). These properties allow piezoelectric transducers to be used as both actuators and sensors and can be represented mathematically by the following linear equations [15]:

$$D = dT + \epsilon^T E \quad (1)$$

$$S = s^E T + dE. \quad (2)$$

In these equations D represents the electrical displacement, S the strain, T the stress, E the applied electric field and the constants d , ϵ^T , s^E represent material properties. The first equation describes the direct and the second the converse piezoelectric effect.

Due to these properties piezoelectric materials have been successfully employed in various applications, especially in

the control of highly resonant flexible structures [31, 9, 2] as well as the emerging field of nanotechnology [29, 3]. Even though these materials have been successfully used in many engineering applications they suffer from a nonlinearity known as hysteresis. This nonlinear phenomenon has been well documented [18, 22] and occurs most frequently when the piezoelectric transducer is used as an actuator and is driven by relatively large voltages. This can be observed by plotting the electric field applied to the transducer versus its displacement (or strain) or vice versa.

1.1. Hysteresis

Hysteresis is the major form of nonlinearity present in piezoelectric transducers. The original meaning of the word refers to ‘lagging behind’ or ‘coming after’; however, it must not be confused with phase lag which is not a nonlinearity and is inherent in most linear systems. These two behaviors can be distinguished by plotting the input and output signals coming in and going out of a system against each other. The hysteretic system will show sharp reversal peaks at its extremum values (figure 1(a)), whereas the tips of a linear system will be more rounded and will display the overall

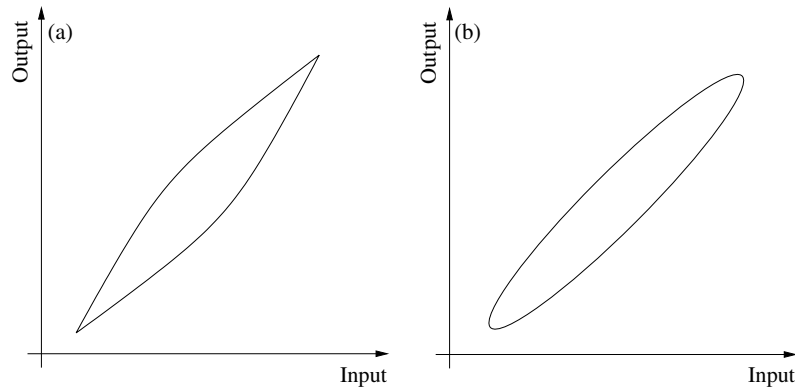


Figure 1. Input–output plots displaying (a) hysteresis and (b) phase lag.

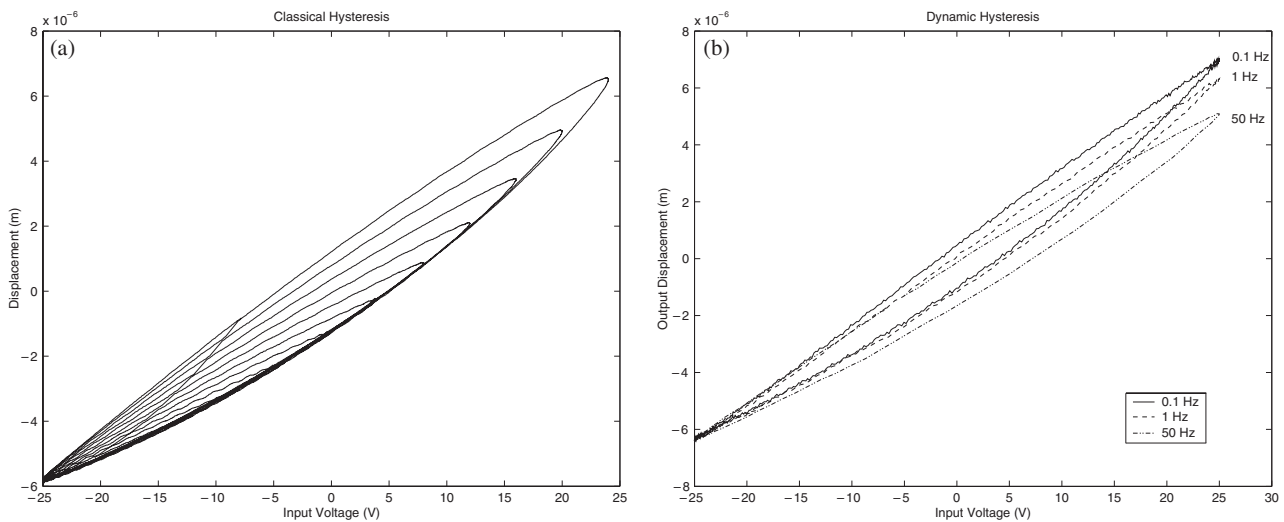


Figure 2. (a) Classical hysteresis, (b) dynamic hysteresis.

shape of an ellipse (figure 1(b)). It is important to note that these two behaviors are not mutually exclusive. In fact they often occur together, especially when the piezoelectric transducer is bonded or attached to a mechanical structure. Nevertheless a clear distinction must be made between the two. The hysteretic distortion does not affect the whole input cycle, but will manifest itself between signal reversals.

The level of hysteretic distortion will also vary depending on either the maximum value of the input voltage being applied (figure 2(a)) or the frequency of the input signal (figure 2(b)) or both¹. This latter case is referred to as ‘dynamic’ or ‘rate dependent’ hysteresis.

On a macroscopic level hysteresis is caused by internal energy losses (or power dissipation) in piezoelectric materials when expanding or contracting. The extent to which a piezoelectric material is susceptible to hysteresis is inversely proportional to its ‘*Q*’ factor [17], or, otherwise stated, the

Q factor is inversely proportional to the power dissipation in a piezoelectric transducer. Large *Q* factor piezoelectric materials, such as quartz, show little or no hysteresis; however they do not have a large electromechanical coupling coefficient and are expensive to produce. The opposite can be said of the piezoelectric ceramic material lead zirconate titanate (PZT), which has a low *Q* factor, large electromechanical coupling and is relatively cheap to manufacture. However, due to their low *Q* factors, PZT transducers display a significant amount of hysteresis.

This phenomenon can cause serious problems in feedback control systems if it is not accounted for when the controller is being designed, since several different output states can be obtained from the same input value depending on the ‘memory’ (or past history) stored in the material. This situation can be avoided by using relatively low voltages; however this prevents the piezoelectric actuators from being used to their maximum potential. Finding a solution to this problem was the motivation for this paper.

To successfully use piezoelectric transducers to their full potential in control schemes, it is essential to accurately understand and model their behavior. Two different approaches are mainly used to model hysteresis in

¹ These plots were obtained at the Laboratory for Dynamics and Control of Smart Structures at the University of Newcastle, Australia, using a PIP-844.60 piezoelectric stack actuator. Graph (a) was obtained by applying a modulated sinusoidal input voltage signal to the stack and measuring its corresponding elongation. Graph (b) was obtained by using a sinusoidal input voltage signal at different frequencies and measuring the corresponding stack elongation.

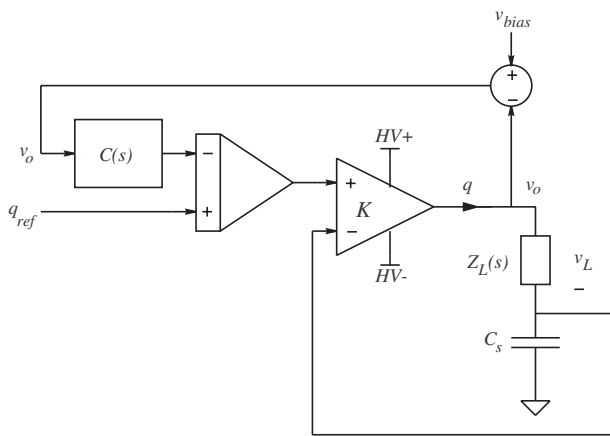


Figure 3. Electrical schematic diagram of a charge amplifier.

piezoelectric materials. The first is the Preisach hysteresis model [24, 15, 13, 27] and the second is the Maxwell resistive capacitor (MRC) model [15, 19, 20]. Each of these operators has been reported to adequately model hysteresis. The inverse of these models is then obtained and subsequently used in a feed forward scheme to compensate for this nonlinearity. The derivation and experimental preparation for these models is somewhat complex and is keeping them from being widely used.

Other methods for dealing with hysteresis have been reported, which avoid the need for an accurate model of the piezoelectric transducer. One such method is the phaser approach developed by Cruz-Hernandez and Hayward [5, 6]. Describing functions have also been implemented with relative success [21, 22].

Another method is to use current or charge sources for the actuation, which has been shown to naturally minimize the effects of hysteresis [21, 1, 28, 4, 12] as well as increase the gain and phase margins of the controlled system [22]. By simply regulating the charge or current a fivefold reduction in hysteresis has been achieved [14, 8]. However, the perceived

implementation complexity of such circuits has prevented their wide acceptance [23]. The main problem is that the circuit offsets often result in the load capacitor being charged up, and if this is not alleviated the compliance voltage will reach the supply rails resulting in a saturated (distorted) output signal. Having an effective means of dealing with these offsets is what has prevented current and charge amplifiers from gaining a wider acceptance.

Recently a solution to this problem has been presented by Fleming and Moheimani [10], in which they use a compliance feedback loop in the current amplifier to estimate and reject all DC offsets (figure 3).

To understand the operation of the system consider the simplified schematic diagram of a compliance feedback charge amplifier shown in figure 3. The high voltage op-amp K works to equate the input q_{ref} to the voltage across the sensing capacitance C_s . The load impedance $Z_L(s)$ experiences a charge q proportional to the input signal q_{ref} . The charge gain of the amplifier is C_s coulombs per volt. The additional feedback loop compensated by $C(s)$, the compliance controller, prevents DC offsets by regulating the output voltage v_o to zero. The signal v_{bias} forces a constant offset voltage (other than zero) across the load. This feature is used for electrical pre-stressing of piezoelectric actuators to allow bi-polar actuation. A more detailed explanation as well as specific information regarding the charge source are provided in [11].

Due to this new development we were able to use a charge source as a means of reducing hysteresis (figure 4) as well as in our control feedback loop for regulating vibrations of highly resonant structures.

2. Modeling

The modeling of our experimental set-up will be carried out in two parts. The first part will deal with the electrical representation of a piezoelectric transducer when used as an actuator and the consequences that arise from using a charge rather than a voltage amplifier. Secondly we will consider the

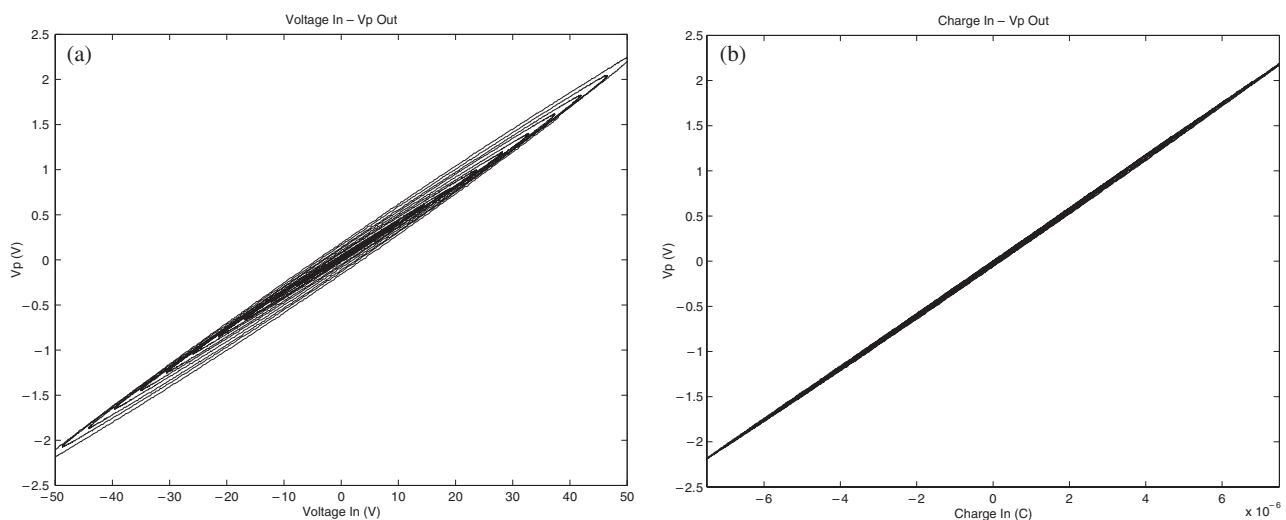


Figure 4. Collocated (a) input voltage and output voltage (displaying hysteresis), (b) input charge and output voltage (reduced hysteresis), using a 24 Hz sinusoidal signal in both cases.

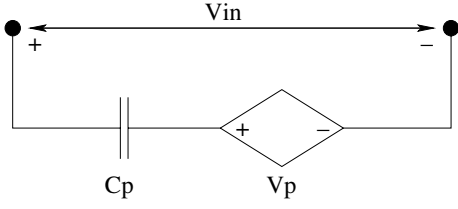


Figure 5. Electrical representation of a piezoelectric transducer.

coupled dynamics of a piezoelectric patch when bonded to a resonant cantilever beam structure.

2.1. Electrical model of a piezoelectric transducer

The ‘linear’ electrical model of a piezoelectric transducer can be represented by a capacitor (C_p) in series with a strain driven voltage source (V_p), as illustrated in figure 5 [7].

Since V_p is directly proportional to the total strain exerted on the piezoelectric transducer, it will give us an indication of the dynamics of the structure it is attached to. Effectively $V_p(t)$ is what allows piezoelectric transducers to act as sensors.

2.1.1. Voltage driven piezoelectric actuator. Traditionally piezoelectric actuators have been driven by voltage and are often collocated with a piezoelectric sensor (figure 6). This arrangement has been widely used in the control of flexible structures as it improves the gain and phase margins of an arbitrary feedback controller.

Let us define the transfer function G_{vv} as the induced voltage across the piezoelectric sensor V_p over the input voltage V_{in} as shown in figure 7 (i.e. $G_{vv} = V_p/V_{in}$). Such collocated transfer functions are easy to distinguish since they always have a zero in between poles. When looking at their Bode plots one can see a peak–trough–peak alternation.

Due to the hysteresis inherent in PZT actuators, the voltage applied across the actuating patch needs to be small to minimize the adverse effect of this nonlinearity.

We can measure G_{vv} by applying a relatively small input voltage (V_a) to the piezoelectric actuator, (therefore minimizing hysteresis), and approximating V_p by measuring the output voltage V_s on the collocated sensor, since V_p cannot be measured directly. G_{vv} can therefore be rewritten as

$$G_{vv}(s) = \frac{V_s(s)}{V_{in}(s)}. \quad (3)$$

Due to the inherent capacitance (C_p) of the piezoelectric sensor it is difficult to obtain accurate measurements of V_s at low frequencies. This can be alleviated by placing a high impedance buffer across the piezoelectric sensor (figure 8). This will ensure that V_p and V_s are identical over the desired bandwidth.

2.1.2. Charge driven piezoelectric actuator. If we now replace the voltage source by a charge source to avoid hysteresis we will obtain a schematic diagram similar to figure 9.

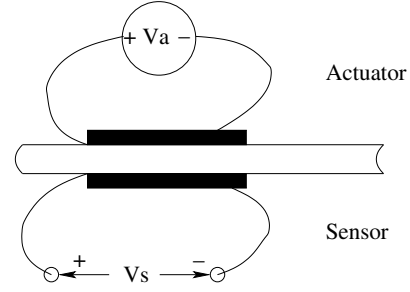


Figure 6. Collocated actuator and sensor pair.

By writing the KVL around the left-hand loop we get

$$V_{in} = \frac{1}{C_p}q - V_p. \quad (4)$$

Let us define G_{vq} as the transfer function from the input charge q to the induced voltage across the piezoelectric sensor V_p ($G_{vq} = V_p/q$).

Since $G_{vv}(s) = V_p(s)/V_{in}(s)$, we can redefine G_{vq} as

$$G_{vq}(s) = \frac{1}{C_p} \left(\frac{G_{vv}(s)}{1 + G_{vv}(s)} \right). \quad (5)$$

This result shows that the poles of G_{vq} are different from those of G_{vv} . Furthermore G_{vq} can be represented by $1/C_p$ in series with a unit feedback loop around G_{vv} as shown in figure 10.

2.2. Coupled piezoelectric–beam modeling

Piezoelectric transducers can be effectively used to reject unwanted vibrations that arise from disturbance forces acting on a flexible structure. These disturbances can generally be represented by point, distributed or moment forces.

In the case of our experiment we looked at regulating the tip displacement of a cantilever beam by using collocated piezoelectric transducers situated close to the clamped end; one is the actuator driven by a charge source and the other is used as a sensor. A moment disturbance will also be applied to the center of the beam by a third PZT patch as illustrated on figure 11.

This problem can be reformulated in block diagram form as shown in figure 12.

We can now compare the voltage and charge driven scenarios in state space form. We will first consider the voltage driven case from which we will derive the charge driven relationship, which will be used to design a feedback controller:

$$\dot{x} = Ax + B_w w + B_v v \quad (6)$$

$$Y_{tip} = C_y x + D_{yw} w + D_{yv} v \quad (7)$$

$$V_p = C_v x + D_{vw} w + D_{vv} v \quad (8)$$

where x represents the state vector of the system, and w and v represent the disturbance and control input voltages respectively.

From figure 12 we have

$$v = -V_p + \frac{1}{C_p}q. \quad (9)$$

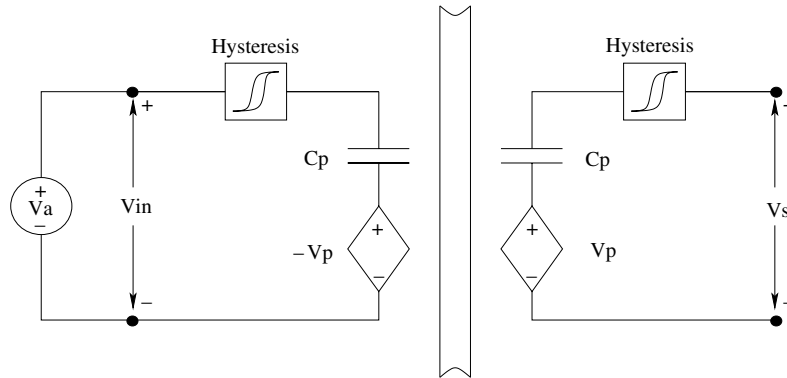


Figure 7. Collocated structure including a hysteresis block driven by a voltage source.

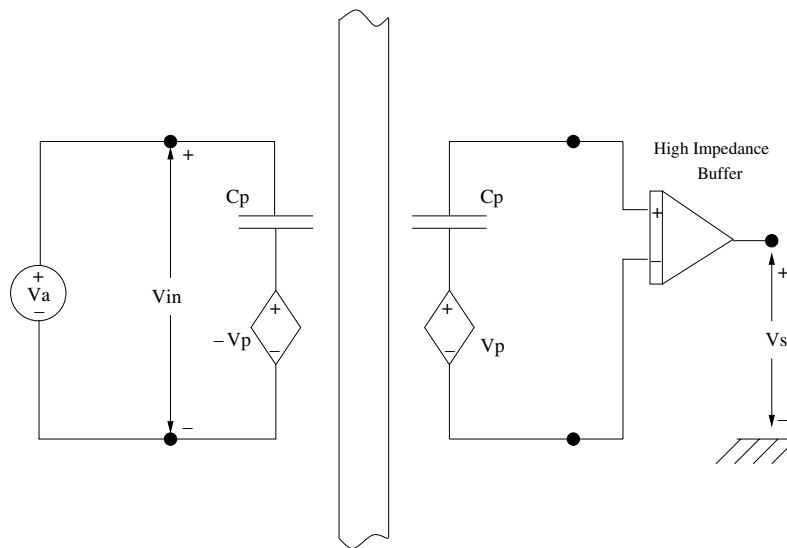


Figure 8. Collocated structure with a high impedance buffer across the piezoelectric sensor.

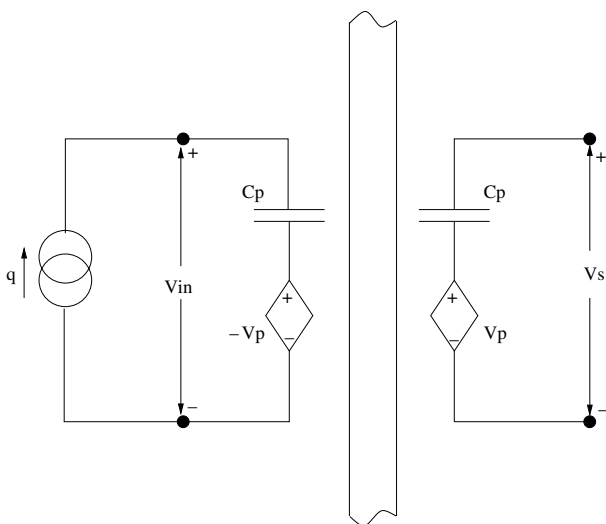


Figure 9. Collocated structure and charge source.

Substituting this back into equations (7) and (8), and rearranging the equations we get the following state space

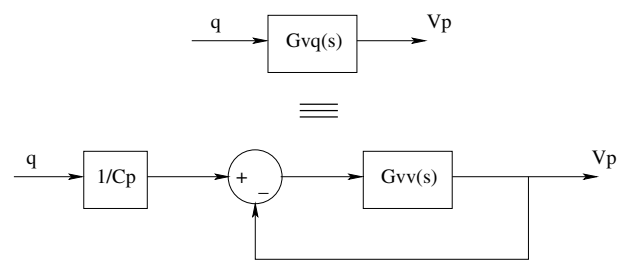


Figure 10. G_{vq} representation in block diagram form.

representation for the charge driven case:

$$\dot{x} = \left(A - B_v \frac{C_v}{1 + D_{vv}} \right) x + \left(B_w - B_v \frac{D_{vw}}{1 + D_{vv}} \right) w + \left(\frac{B_v}{C_p(1 + D_{vv})} \right) q \quad (10)$$

$$Y_{tip} = \left(C_y - D_{yv} \frac{C_v}{1 + D_{vv}} \right) x + \left(D_{yw} - D_{yv} \frac{D_{vw}}{1 + D_{vv}} \right) w + \left(\frac{D_{yv}}{C_p(1 + D_{vv})} \right) q \quad (11)$$

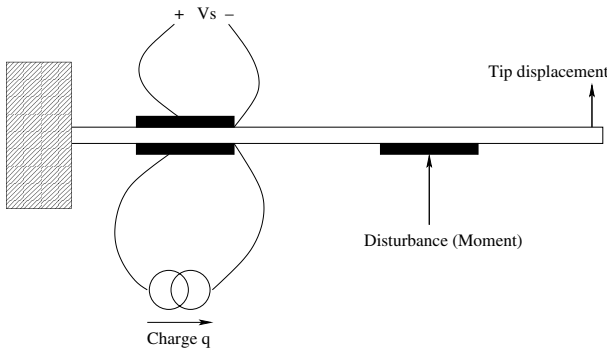


Figure 11. Beam arrangement.

$$V_p = \left(C_v - D_{vv} \frac{C_v}{1 + D_{vv}} \right) x + \left(D_{vw} - D_{vv} \frac{D_{vw}}{1 + D_{vv}} \right) w + \left(\frac{D_{vv}}{C_p(1 + D_{vv})} \right) q. \quad (12)$$

More simply we can write equations (10), (11) and (12) as

$$\dot{x} = A^q x + B_w^q w + B_v^q q \quad (13)$$

$$Y_{tip} = C_y^q x + D_{yw}^q w + D_{yq}^q q \quad (14)$$

$$V_p = C_v^q x + D_{vw}^q w + D_{vq}^q q. \quad (15)$$

We can clearly see from the above equations that the dynamics of the beam have been changed now that we are using charge instead of voltage to drive the collocated actuator (since the A matrices in equations (6) and (10) are different).

To illustrate this we measured the transfer function G_{dw} from input disturbance (w) to tip displacement (Y_{tip}) with the charge amplifier set to zero (i.e. $q = 0$ in equations (13) and (14)) and then a second measurement with the voltage source set to zero (i.e. $v = 0$ in equations (6) and (7)).

The results (figure 13) demonstrate that the poles of the system are indeed different. This is especially obvious for the first two plots. The third plot displays a wider frequency range, which is not as ‘focused’ as the other two and therefore makes it harder to judge.

The plots were obtained by taking the average of eight frequency responses for each scenario.

2.2.1. Analytical model. The physical modeling for this set-up is well understood [16, 25] and uses derivations from the Euler–Bernoulli beam equation to determine the transfer function from input voltage (v) to output voltage (V_s) (or output tip displacement Y_{tip}).

From these derivations it has been shown that the A , B and C matrices (for the voltage driven case) are of the form

$$A = \begin{bmatrix} 0 & 1 & 0 & 0 \\ -\omega_1^2 & -2\zeta_1\omega_1 & 0 & 0 \\ & & \ddots & \\ 0 & 0 & 0 & 1 \\ 0 & 0 & -\omega_i^2 & -2\zeta_i\omega_i \end{bmatrix} \quad (16)$$

$$B = [B_w \quad B_v] = \begin{bmatrix} 0 & H_1^w & \cdots & 0 & H_i^w \\ 0 & H_1^v & \cdots & 0 & H_i^v \end{bmatrix}^T \quad (17)$$

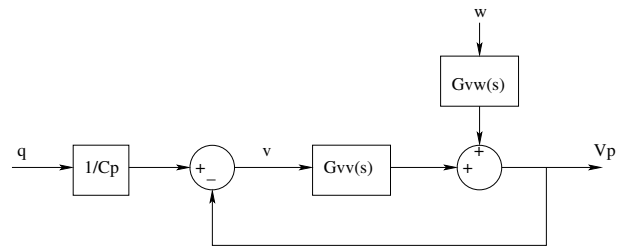


Figure 12. Beam arrangement in block diagram form.

$$C = [C_y \quad C_v]^T = \begin{bmatrix} F_1^y & 0 & \cdots & F_i^y & 0 \\ F_1^v & 0 & \cdots & F_i^v & 0 \end{bmatrix} \quad (18)$$

where ω_i and ζ_i correspond to the natural frequency and damping ratio for each i th vibrational mode, H_i^w and H_i^v are values that correspond to the input disturbance (w) and control input voltage (v), respectively, and F_i^y and F_i^v are values that correspond to the output tip displacement and induced output voltage respectively. These matrices (A , B and C) are then used in equations (10), (11) and (12) to determine the charge driven matrices A_q , B_q , C_q and D_q .

In our experiment we only considered the first three vibrational modes of the beam. We therefore had to include a feed-through term D to compensate for the misalignment of the in-bandwidth zero locations that arise from not modeling the higher order modes [26].

To determine these parameters we built a two-input (charge q and disturbance w), two-output (induced voltage V_p and tip displacement Y_{tip}) plant (figure 14) and used an optimization procedure (using the simplex search algorithm ‘fminsearch’ in MATLAB) to minimize the function:

$$M = \sum |R_{yw} - R_{yw}^m| + \sum |R_{yq} - R_{yq}^m| + \sum |R_{vw} - R_{vw}^m| + \sum |R_{vq} - R_{vq}^m| \quad (19)$$

where R_{yw} , R_{yq} , R_{vw} and R_{vq} correspond to the complex frequency responses of the model described by equations (10), (11), (12), and R_{yw}^m , R_{yq}^m , R_{vw}^m and R_{vq}^m correspond to the complex frequency responses of the measured experimental data. The calculated and measured frequency responses must be evaluated at the same frequency points.

The authors have found that it is best to fix the values of ω and ζ for each mode, before performing the optimization. This means that only the H and F values of the B and C matrices, as well as the values of the D matrix, need to be determined using the simplex algorithm.

The natural frequencies ω and damping ratios ζ for each mode can be obtained and fine-tuned by trial and error by measuring the location and height of the peaks from the measured Bode plot frequency responses. Equation (19) was also slightly modified to weight certain frequency regions more heavily to obtain better zero locations.

The results from using this procedure are illustrated in figure 15, and show that the identified model closely matches the experimentally measured data.

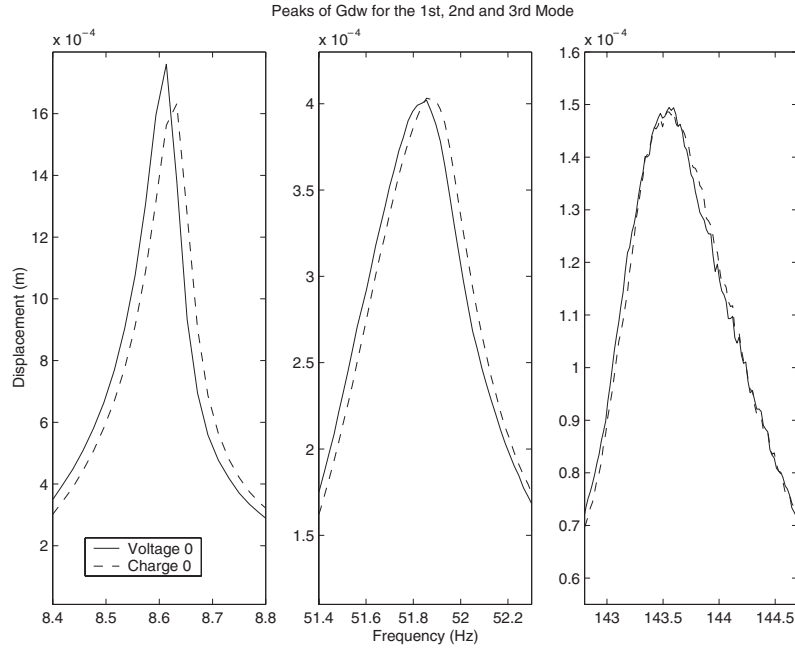


Figure 13. Peaks of G_{dw} showing the first, second and third modes, when the control signal is set to zero for the voltage and charge case.



Figure 14. Augmented MIMO plant.

3. Controller design

With the identified model a controller can be designed to minimize the tip displacement of the beam. However more than just minimizing a given cost function we must ensure that the controller will shift the closed loop poles of the system further to the left in the complex plane. This will guarantee that the closed loop system is more highly damped and therefore less sensitive to external disturbances no matter where they act on the system.

The feedback controller $C(s)$ will be obtained by combining a LQR state feedback controller K_q and a Kalman state observer O , as depicted in figure 16. By the certainty equivalence principle [30] the optimum regulator K_q and observer O can be determined independently.

3.1. LQR controller design

Our design objective is to minimize the beam tip displacement (Y_{tip}) as well as to keep the control input (q) below saturation. Saturation will occur if the required control signal is greater than the rail voltage supplied to the charge amplifier, which in our case was ± 30 V.

In a linear quadratic sense we want to minimize

$$J = \int_0^{\infty} \{Y_{tip}^2(t) + q'(t)k_u q(t)\} dt \quad (20)$$

where k_u is a weighting scalar on the applied charge control signal q . On the basis of our state space model of the plant (14), Y_{tip} is equal to

$$Y_{tip} = C_y^q x + D_{yw}^q w + D_{yq}^q q.$$

Since we will be looking at the deterministic linear quadratic regulator (LQR) problem we can remove the process noise [30], and therefore rewrite Y_{tip} as

$$Y_{tip} = C_y^q x + D_{yq}^q q. \quad (21)$$

In practice D_{yq}^q is negligible. Substituting (21) (with $D_{yq}^q = 0$) into (20) and rearranging the terms, we finally arrive at the standard LQR deterministic cost function:

$$J = \int_0^{\infty} \{x'(t)Qx(t) + q'(t)Rq(t)\} dt \quad (22)$$

where

$$Q = C_y^{q'} C_y^q$$

$$R = k_u.$$

Q and R represent the performance and controller input weightings respectively. To effectively reduce the tip displacement we chose $Q = \tilde{C}_y' \tilde{C}_y$, where \tilde{C}_y is equal to C_y with different weightings on each mode to dampen them by the same amount:

$$\tilde{C}_y = C_y \begin{bmatrix} 2 & & & & \\ & 2 & & & 0 \\ & & 10 & & \\ & & & 10 & \\ 0 & & & & 25 \\ & & & & & 25 \end{bmatrix}. \quad (23)$$

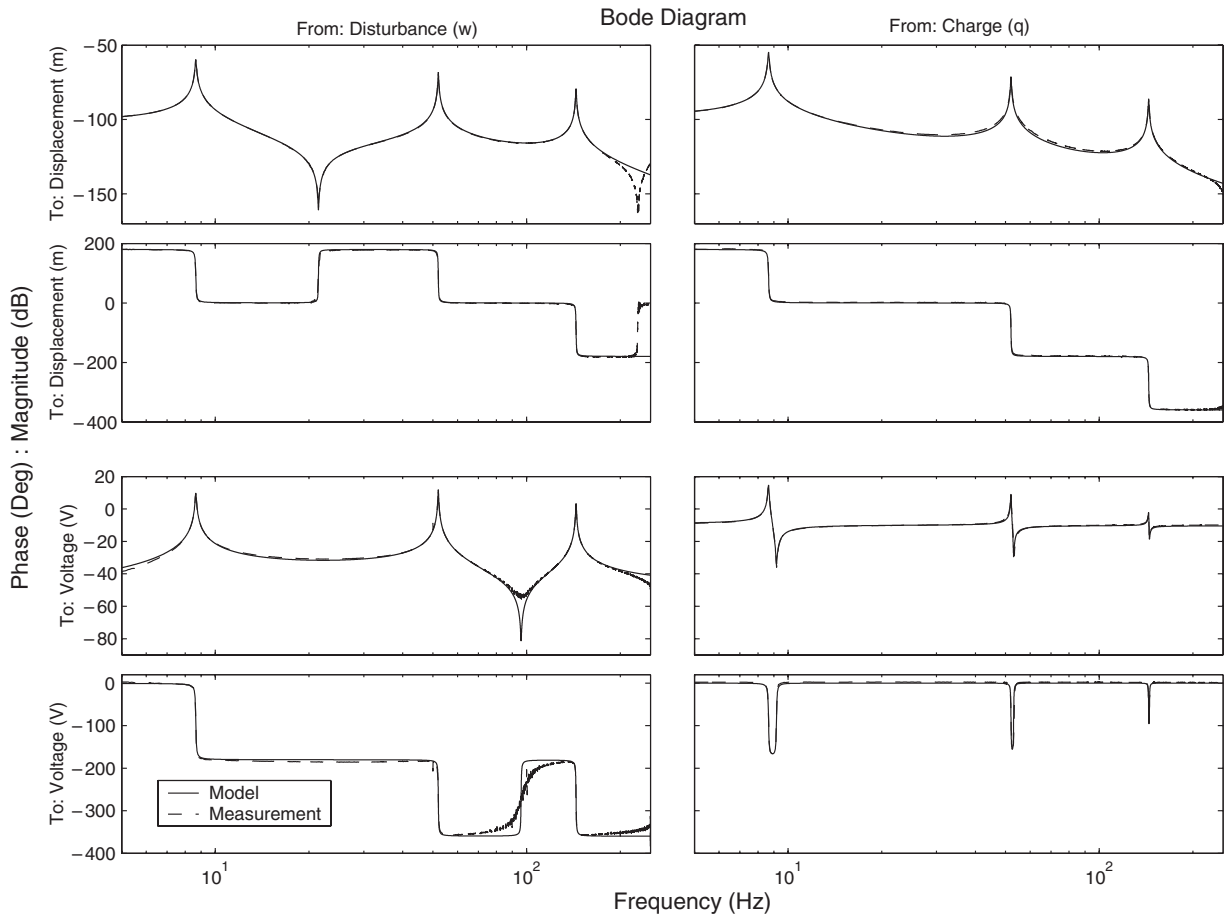


Figure 15. Identified model with measured data.

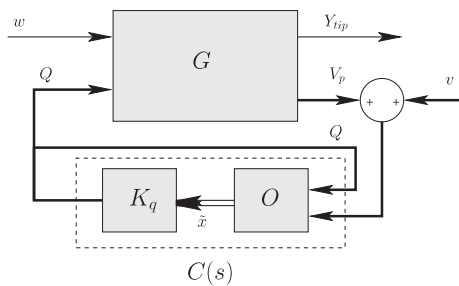


Figure 16. Feedback controller $C(s)$ including state feedback controller K_q and state observer O .

The values for C_y are given here in order to illustrate the fact that by using a structured model of the plant (section 2.2.1), the weightings for each mode can be determined easily and that there is a correlation between the weighting value and the natural frequency of the corresponding mode.

The optimum state feedback controller K_q that minimizes J is obtained by solving the corresponding algebraic Riccati equation [30].

3.2. Kalman observer

Since we are only measuring the voltage sensor V_p we need to design an observer to estimate the states of the plant. To

achieve this we designed a Kalman observer O to minimize

$$J_o = E \left\{ [x(t) - \tilde{x}(t)]' [x(t) - \tilde{x}(t)] \right\} \quad (24)$$

where x and \tilde{x} are the exact and estimated states of the plant respectively and E is the expectation operator.

We also made the following assumptions: that the disturbance (w) and the measurement noise (v) (cf figure 16) are uncorrelated zero-mean Gaussian stochastic processes with constant power spectral density matrices W and V respectively. Therefore the covariances of w and v are

$$E \{ w(t)w'(t) \} = W \quad (25)$$

$$E \{ v(t)v'(t) \} = V \quad (26)$$

and

$$E \{ w(t)v'(t) \} = 0, \quad E \{ v(t)w'(t) \} = 0. \quad (27)$$

A Kalman observer O that minimizes (24) can then be found by solving an algebraic Riccati equation, which is based on W and V [30]. The observer is then coupled to the state feedback controller K_q to form the controller $C(s)$, which was used in our experiments.

In this work W and V and R are simply used as design parameters, which are fine-tuned to obtain adequate closed loop pole locations.

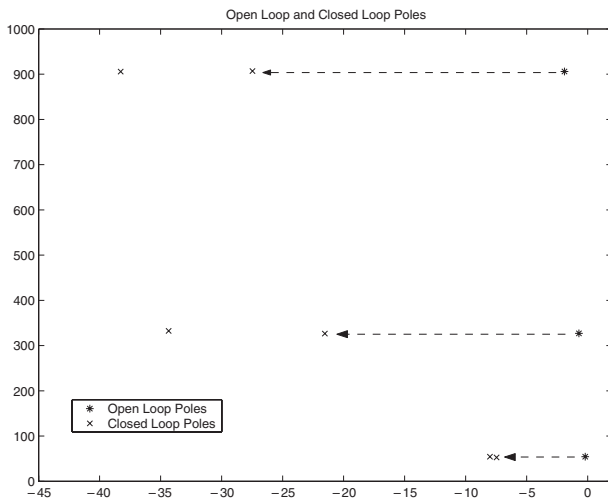


Figure 17. Open loop and closed loop poles of the system.

To measure the effectiveness of this controller the open loop and closed loop poles of the plant were compared in figure 17. Only the second quadrant is shown for clarity. This clearly demonstrates that extra damping has been added to the system. This is important since there would be situations where we would not know exactly where the disturbance is entering the system. However, by ensuring that the poles of the closed loop system are significantly damped, the disturbance can act anywhere along the beam and yet the tip displacement will be significantly less than without the feedback controller.

4. Experimental results

The experiments were performed at the Laboratory for Dynamics and Control of Smart Structures at the University of Newcastle, Australia. The experiments were carried out on a cantilever Euler beam with identical collocated PIC 151 piezoelectric patches, with dimensions and properties shown in figure 18, tables 1 and 2. A physical picture of the beam is shown in figure 19 (even though the picture shows three patches, only the two closest to the clamped end were used). The disturbance voltage was applied to a secondary patch located at the center of the beam and the collocated actuator-sensor pair was used as the control feedback structure to reject the output disturbances (or as we have seen in the previous section to effectively add damping to the beam). A Polytec

Table 1. Beam properties.

Length, L	550 mm
Thickness, h	3 mm
Width, W	50 mm
Density, ρ	$2.77 \times 10^3 \text{ m V}^{-3}$
Young's mod., E	$7.00 \times 10^{10} \text{ N m}^{-2}$

Table 2. PIC 151 Ceramic properties. (Manufactured by Physik Instrumente (PI) GmbH and Co. KG.)

Length, L_{pz}	50 mm
Thickness, h_{pz}	0.25 mm
Thickness (disturbance), h_{pz_d}	0.50 mm
Width, W_{pz}	25 mm
Charge constant, d_{31}	$-210 \times 10^{-12} \text{ m V}^{-1}$
Voltage constant, g_{31}	$-11.5 \times 10^{-3} \text{ V m N}^{-1}$
Coupling coefficient, k_{31}	0.34
Capacitance, C_p^S	115 nF

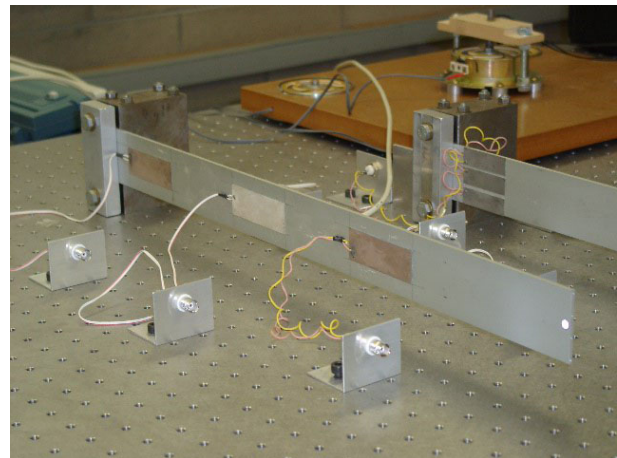


Figure 19. Picture of the physical beam.

(This figure is in colour only in the electronic version)

laser scanning vibrometer (PSV-300) was used to measure the velocity at the tip of the beam.

The frequency responses were obtained by applying a sinusoidal voltage signal of varying frequency to the 'disturbance' piezoelectric patch and measuring the corresponding output signals of interest (namely the output voltage V_p from the collocated sensors and the output displacement at the tip of the beam Y_{tip}) with and without the controller being switched on. Given the input

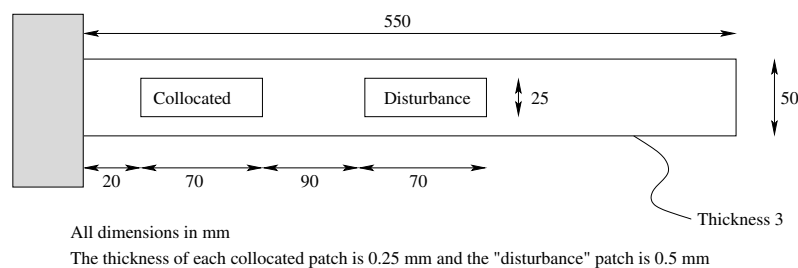


Figure 18. Beam set-up and dimensions.

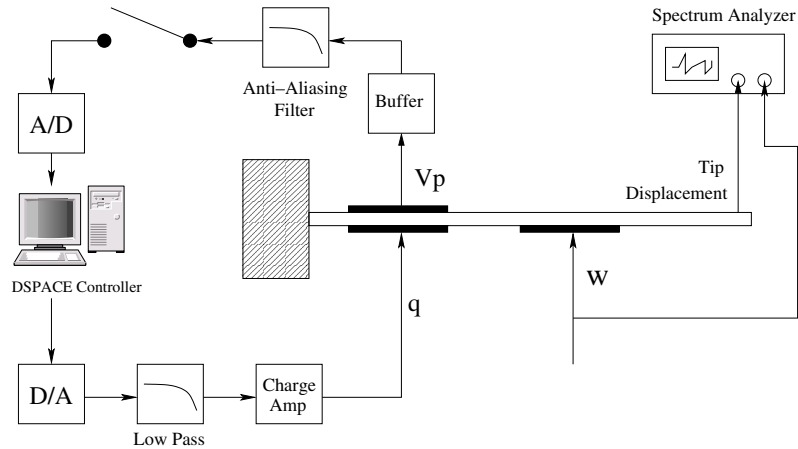


Figure 20. Experimental schematic diagram.

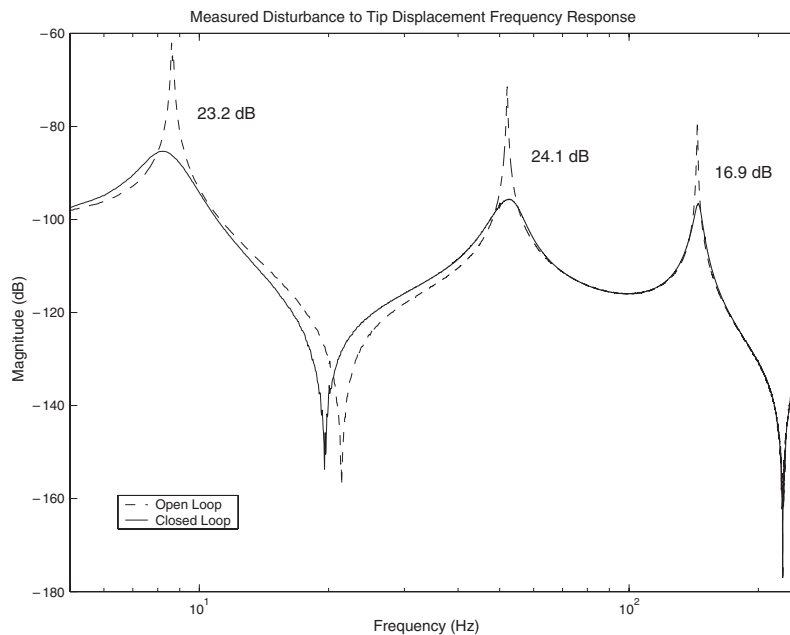


Figure 21. Measured open and closed loop frequency response for input disturbance w to output tip displacement Y_{tip} .

and output signals the spectrum analyzer will compute the corresponding frequency response.

The controller was downloaded from Simulink onto a DSpace 1103 DSP board. We used a low pass filter to remove the high frequency content introduced by the D/A converter as well as an anti-aliasing filter for the measured ‘sensor’ signal. The schematic diagram of the arrangement is given in figure 20. A high impedance buffer, which is comprised of a voltage divider and an instrumentation amplifier, was also used to keep the phase of the ‘sensor’ signal from increasing at low frequencies.

The results obtained with the charge controller were very satisfactory. We measured the transfer function G_{yw} (input disturbance to output tip displacement Y_{tip}) with and without the charge controller, using the Polytec spectrum analyzer. These plots are shown in figure 21. The simulated results for G_{yw} are shown in figure 22. One can see that the simulation results closely match the experimental measurements.

We also measured the velocity step response at the tip of the beam, using the Polytec laser scanning vibrometer. These results were obtained by introducing a low pass filtered (250 Hz) step signal through the disturbance channel. The displacement step response was obtained by integrating the velocity response (figure 23).

5. Conclusion

In this paper we have shown that electrical charge can be used to drive piezoelectric actuators for the purpose of vibration control. The motivation for this approach is to reduce negative effects associated with hysteresis, which can become significant when a piezoelectric actuator is driven by a voltage amplifier. By using charge we are able to obtain a more accurate model of the plant, which can then be used to design a more robust or better performing feedback controller. During our analysis we have also demonstrated that the dynamics

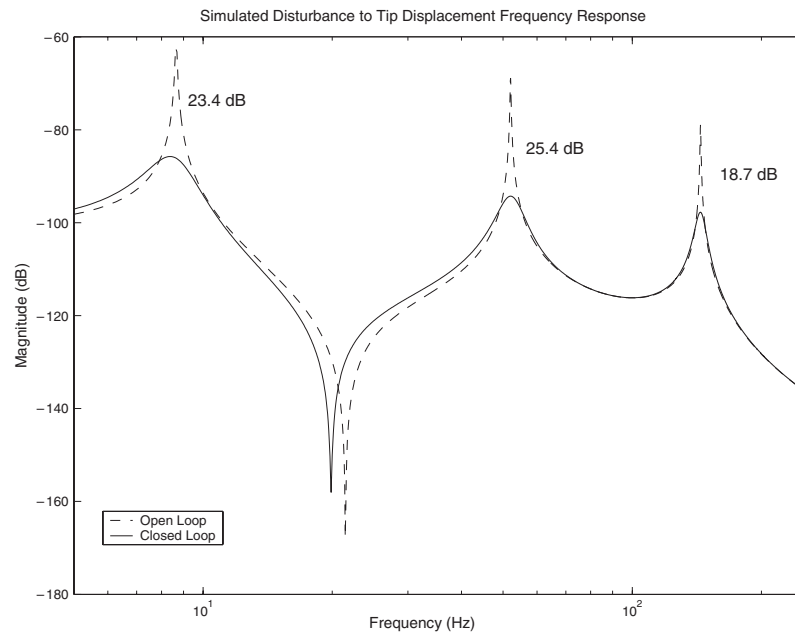


Figure 22. Simulated open and closed loop frequency response for input disturbance w to output tip displacement Y_{tip} .

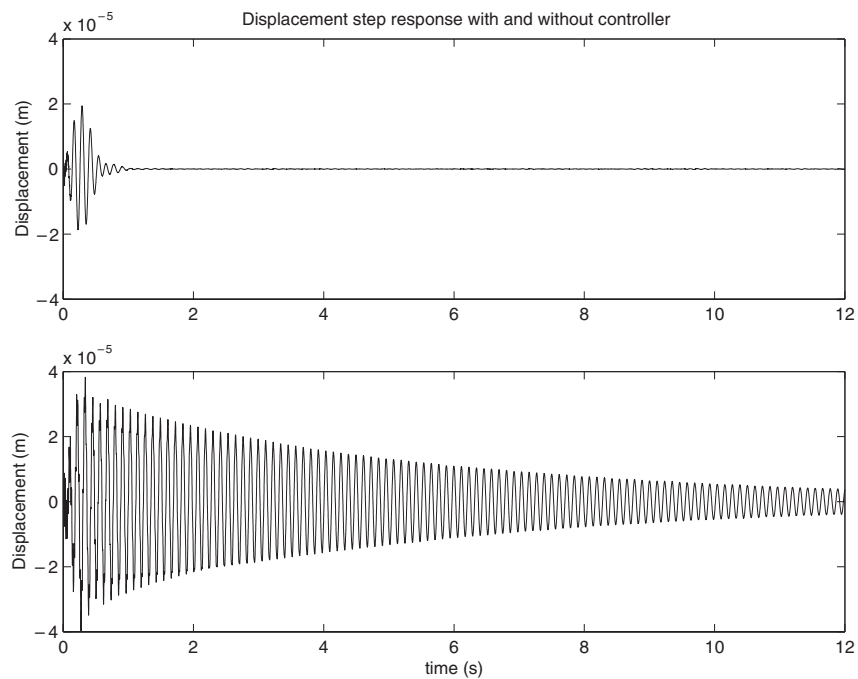


Figure 23. Displacement step response at the tip of the beam with and without a controller.

(i.e. the poles) for the coupled ‘piezoelectric–beam’ system differs depending on whether electrical charge or voltage is used to drive the piezoelectric actuator. Therefore care must be taken when modeling the plant as this will affect the design of the feedback controller. The authors will be looking at extending this approach to MIMO systems.

Acknowledgments

This research was supported by the Australian Research Council and the Center for Complex Dynamic Systems and Control.

References

- [1] Adriaens H J, de Koning W L and Banning R 2000 Modeling piezoelectric actuators *IEEE/ASME Trans. Mechatron.* **5** 331–41
- [2] Behrens S, Fleming A J and Moheimani S O R 2003 A broadband controller for piezoelectric shunt damping of structural vibration *Smart Mater. Struct.* **12** 18–28
- [3] Bonnail N, Tonneau D, Capolino G A and Dallaporta H 2000 Dynamic and static responses of a piezoelectric actuator at nanometer scale elongations *Proc. IEEE Ind. Appl. Conf.* **1** 293–8

- [4] Comstock R H 1981 Charge control of piezoelectric actuators to reduce hysteresis effects *US Patent Specification* 4263527
- [5] Cruz-Hernandez J M and Hayward V 1998 An approach to reduction of hysteresis in smart materials *Proc. IEEE Int. Conf. Robot. Automat.* pp 1510–5
- [6] Cruz-Hernandez J M and Hayward V 2001 Phase control approach to hysteresis reduction *IEEE Trans. Control Syst. Technol.* **9** 17–26
- [7] Dosch J J, Inman D J and Garcia E 1992 A self-sensing piezoelectric actuator for collocated control *J. Intell. Mater. Syst. Struct.* **3** 165
- [8] Takata K *et al* 1989 Piezoelectric actuator control apparatus *US Patent Specification* 4841191
- [9] Fleming A J, Behrens S and Moheimani S O R 2002 Optimization and implementation of multimode piezoelectric shunt damping systems *ASME/IEEE Trans. Mechatron.* **7** 87–94
- [10] Fleming A J and Moheimani S O R 2003 Precision current and charge amplifiers for driving highly capacitive piezoelectric loads *IEE Electron. Lett.* **39** 282–4
- [11] Fleming A J and Moheimani S O R 2004 Improved current and charge amplifiers for driving piezoelectric loads, and issues in signal processing design for synthesis of shunt damping circuits *J. Intell. Mater. Syst. Struct.* **15** 77–92
- [12] Furutani K, Urushibata M and Mohri N 1998 Displacement control of piezoelectric element by feedback of induced charge *Nanotechnology* **9** 93–8
- [13] Ge P and Jouaneh M 1995 Modeling hysteresis in piezoceramic actuators *Precision Eng.* **17** 211–21
- [14] Ge P and Jouaneh M 1996 Tracking control of a piezoceramic actuator *IEEE Trans. Control Syst. Technol.* **4** 209–16
- [15] Goldfarb M and Celanovic N 1997 A lumped parameter electromechanical model for describing the nonlinear behavior of piezoelectric actuators *J. Dyn. Syst. Meas. Control* **119** 478–85
- [16] Halim D and Moheimani S O R 2001 Spatial resonant control of flexible structures—application to piezoelectric laminate beam *IEEE Trans. Control Syst. Technol.* **9** 37–53
- [17] Kelly J, Ballato A and Safari A 1996 The effect of a complex piezoelectric coupling coefficient on the resonance and antiresonance frequencies of piezoelectric ceramics *Proc. 10th IEEE Int. Symp. on Applications of Ferroelectrics* vol 2 (Piscataway, NJ: IEEE) pp 825–8
- [18] Koops K R, Scholte P M L O and de Koning W L 1999 Observation of zero creep in piezoelectric actuators *Appl. Phys.* **68** 691–7
- [19] Lee S H and Royston T J 2000 Modeling piezoceramic transducer hysteresis in the structural vibration control problem *J. Acoust. Soc. Am.* **108** 2843–55
- [20] Lee S H, Royston T J and Friedman G 2000 Modeling and compensation of hysteresis in piezoceramic transducers for vibration control *J. Intell. Mater. Syst. Struct.* **11** 781–90
- [21] Main J A and Garcia E 1997 Design impact of piezoelectric actuator nonlinearities *AIAA J. Guid. Control Dyn.* **20** 327–32
- [22] Main J A and Garcia E 1997 Piezoelectric stack actuators and control system design: strategies and pitfalls *AIAA J. Guid. Control Dyn.* **20** 479–85
- [23] Main J A, Garcia E and Newton D V 1995 Precision position control of piezoelectric actuators using charge feedback *AIAA J. Guid. Control Dyn.* **18** 1068–73
- [24] Mayergoyz I 1991 *Mathematical Models of Hysteresis* (Berlin: Springer)
- [25] Meirovitch L 1975 *Elements of Vibration Analysis* (New York: McGraw-Hill)
- [26] Moheimani S O R 2000 Minimizing the effect of out-of-bandwidth dynamics in the models of reverberant systems that arise in modal analysis: implications on spatial \mathcal{H}_∞ control *Automatica* **36** 1023–31
- [27] Mrad R B and Hu H 2002 A model for voltage to displacement dynamics in piezoceramic actuators subject to dynamic voltage excitations *IEEE/ASME Trans. Mechatron.* **7** 479–89
- [28] Newcomb C V and Flinn I 1982 Improving the linearity of piezoelectric ceramic actuators *Electron. Lett.* **18** 442–3
- [29] Salapaka S, Sebastian A, Cleveland J P and Salapaka M V 2002 Design, identification and control of a fast nanopositioning device *Proc. Am. Control Conf.* pp 1966–71
- [30] Skogestad S and Postlethwaite I 1996 *Multivariable Feedback Control* (New York: Wiley)
- [31] Tsai M S and Wang K W 1999 On the structural damping characteristics of active piezoelectric actuators with passive shunt *J. Sound Vib.* **221** 1–22